THE JOURNAL OF PHYSICAL CHEMISTRY B

Article

pubs.acs.org/JPCB

Induced Dipoles Incorporated into All-Atom Zn Protein Simulations with Multiscale Modeling

Yan-Dong Huang[†] and Jian-Wei Shuai*[,†,‡]

[†]Department of Physics and Institute of Theoretical Physics and Astrophysics, Xiamen University, Xiamen 361005, China

[‡]Fujian Provincial Key Laboratory of Theoretical and Computational Chemistry, Xiamen University, Xiamen 361005, China

Supporting Information

ABSTRACT: Zinc is found saturated in the deposited Amyloid-beta ($A\beta$) peptide plaques in Alzheimer's disease (AD) patients' brains. Binding of zinc promotes aggregation of $A\beta$, including the pathogenic aggregates. Up to now, only the region 1−16 of $A\beta$ complexed with zinc ($A\beta_{1-16}$−Zn) is defined structurally in experiment. In order to explore the induced polarization effect of zinc on the global fluctuations and the experimentally observed coordination mode of $A\beta_{1-16}$−Zn, we consider an all-atom molecular dynamics (MD) of $A\beta_{1-16}$−Zn solvated in implicit water. In our model, the zinc polarization affects the whole peptide. The induced dipoles are divided into three distinct scales according to their distances from zinc. Besides, the atomistic polarizability on the coordinating side chains is rescaled to describe the electron redistribution effect. We show that, associated with proper van der Waals (vdW) parameters, our model not only obtains the reasonable coordinating configuration of zinc binding site but also retains the global stabilization, especially the N-terminal region, of the $A\beta_{1-16}$−Zn. We suggest that it is the induced polarization effect that promotes reasonable solvent exposures of hydrophobic/hydrophilic residues regarding zinc-induced $A\beta$ aggregation.

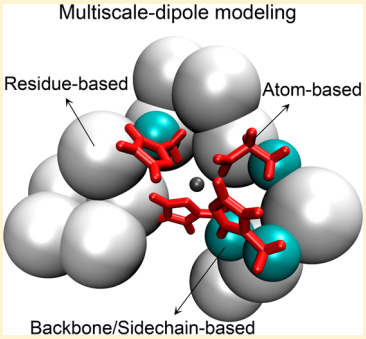

1. INTRODUCTION

Alzheimer's disease (AD) is a fatal neurodegenerative disorder and characterized by aggregation of amyloid-beta peptide ($A\beta$) into insoluble plaque in AD patient brains. Zinc is found with high concentration in the plaque.[1] It is believed that zinc plays a key role in $A\beta$-related pathogenesis of AD.[2−10] Zinc binding sites are critical for the functions and/or structural organizations of folded zinc proteins. Thus, most current theoretical models focus on the effect of zinc within the coordination shell. However, for unstructured peptides (i.e., $A\beta$), an accurate and efficient theoretical simulation method is required to investigate the global impact of zinc on peptides.

Considering an accurate description of zinc binding site interactions, the first-principal MD method or hybrid quantum mechanics/molecular mechanics MD method (QM/MM MD) has been recently used to study the local/global conformation fluctuations of truncated $A\beta$−Zn complex.[11,12] Nevertheless, $A\beta$ has been demonstrated to be an intrinsically disordered peptide,[13−15] so it is not sufficient to account for the impact of zinc on $A\beta$ in a local domain or small time scale. For example, the 11th amino acid (a.a.) residue (Glu11) of $A\beta$ experimentally displays a bidentate binding fashion.[16] However, the QM-based models suggest a monodentate binding to zinc,[11,12] which might be due to the lack of correct description of the protein environment. In order to improve the quality of conformational sampling, more extensive interactions between zinc and $A\beta$ should be taken into account. However, computational studies of the biomolecular structures in the framework of quantum mechanics schemes are often hampered by extremely demanding computer time.

On the other hand, classical molecular dynamics methods with a variety of force fields have been developed to study the global/local conformational fluctuations of zinc proteins in a larger time scale with more extensive samplings.[17−22] However, most of the current empirical force fields do not explicitly incorporate the effects of zinc-induced polarization and charge transfer, which are both essential for an accurate description of interactions in the zinc binding site.[23−25] Alternatively, coordination bonds and/or angles can be constrained to their NMR evaluated values during the theoretical simulations. This approach has been applied in the studies on the conformations of $A\beta$ monomers and oligomers upon zinc binding.[26−28]

On the basis of the nonbonded model presented by Stote and Karplus,[17] Sakharov and Lim additionally consider the two induction effects, namely, the local polarization effect presented with the atom-based point dipole model and the charge transfer effect specified by updating charges of coordinating atoms and zinc with time during simulations.[23,29] As a complete description of atom−atom interaction, their potential energy function includes all energy components derived from the well-known Kitaura−Morokuma energy decomposition.[30] They presented the induced dipoles at atom-based level which are

Received: March 4, 2013
Revised: April 18, 2013
Published: April 30, 2013

only applied to the first-shell ligands of the zinc binding site for zinc finger proteins.[23]

It has been pointed out that most zinc binding sites can be classified to be either structural or catalytic.[31,32] On the basis of a statistical survey of zinc proteins, if there is no more than one Cys out of the ligating a.a. residues, the zinc binding site is defined to be catalytic.[31] Accordingly, the zinc binding site in $A\beta$, including three histidines and the fourth non-Cys coordinating candidate, belongs to the catalytic site, while it is a structural site in zinc finger proteins. The ligands transfer a lesser amount of charges in most catalytic sites than in structural sites, enabling zinc to serve as a Lewis acid. As a consequence, the charge-dependent polarization capacity of zinc in catalytic sites is generally stronger than that in structural sites.[31] In fact, it has been noted that those residues (i.e., Arg5 and Gly9 in $A\beta$) relatively far from zinc are also polarized.[11] Therefore, it is necessary to account for the global impact of zinc-induced polarization force on $A\beta$ in the MD simulation.

In this paper, we study the 1−16 region of $A\beta$ complexed with zinc ($A\beta_{1-16}$−Zn),[16] in which the 6−14 region is considered the minimal zinc binding domain of $A\beta$.[12] Different from the strategies outlined by Sakharov and Lim,[23] we consider zinc-induced dipoles covering the whole peptide, which are simulated at three resolutions, ranging from the residue-based level, to the intermediate level, and to the atom-based level. With atom-based dipoles applied to the zinc binding site, some atomic information related to zinc binding site, such as the coordination bond length and number, can be studied. With the multiscale dipoles applied to the whole peptide, the computational cost increases linearly only with the a.a. residue number. Besides the polarization effect, charge transfer is also taken into account in our MD method for $A\beta$−Zn discussion. As suggested by Sakharov and Lim, a linear approximation is employed here to calculate the distance-dependent charge transfer from each ligating atom to zinc.[23]

Our MD method has been assessed upon several statistical properties, such as root-mean-square deviations from the experimental structure, radius of gyration, coordinating bond length, and hydrogen bonds involved in the secondary structure of interest. In addition, the solvent-accessible surface area of individual residue is also recorded to explore solvent exposure of a.a. residues. In the end, our method is applied to another zinc complex also with a catalytic-type zinc binding site. The results show that our method is able to reproduce the coordinating configuration as well as the global stabilization of $A\beta_{1-16}$−Zn, which is compatible with experimentally determined structures.

2. METHODS

In this work, the potential energy function that describes the interaction between zinc and $A\beta_{1-16}$ peptide consists of electrostatic polarization force, the Coulomb force, and vdW force, which is given by

$$V_{\mathrm{Zn,Protein}} = V^{\mathrm{pol}} + \sum_i \left\{ \frac{(q^0_{\mathrm{Zn}} + \sum_i \Delta q_{i\to\mathrm{Zn}})(q_i^{\,0} - \Delta q_{i\to\mathrm{Zn}})}{4\pi\varepsilon_0 r_{\mathrm{Zn},i}} + 4\varepsilon_{\mathrm{Zn},i}\left[\left(\frac{R_{\mathrm{Zn},i}}{r_{\mathrm{Zn},i}}\right)^{12} - 2\left(\frac{R_{\mathrm{Zn},i}}{r_{\mathrm{Zn},i}}\right)^{6}\right]\right\} \quad (1)$$

The formula is similar as the conservational nonbonded model,[17] except for an additional term, the electrostatic polarization energy V^{pol}. The initial charges, q^0_{Zn} and q^0_i, of zinc and peptide atoms are extracted from the CHARMM22 force field. The charge transfer effect is incorporated by adjusting charges on zinc and its coordinating atoms at any time step during simulations. $\Delta q_{i\to\mathrm{Zn}}$ is the charge transferred from the ith protein atom to zinc, while $\sum_i \Delta q_{i\to\mathrm{Zn}}$ is the summation of charges transferred from protein atoms to zinc. In practice, only those atoms that directly form coordinating bonds with zinc donate charges.

2.1. Charge Transfer Estimations. The amount of charges transferred to zinc is estimated only from the four amino acids (His6, Glu11, His13, and His14) of $A\beta_{1-16}$. Three neutral histidines and one negatively charged glutamic acid are modeled, respectively, by three imidazole rings (IMI) and one formate ($HCOO^-$) that tetra-coordinated to zinc ($[Zn^{2+}(IMI)_3HCOO^-]^{1+}$). The initial structure of the complex $[Zn^{2+}(IMI)_3HCOO^-]^{1+}$ is extracted from the NMR structure (PDB ID: 1ZE9)[16] and fully optimized at the B3LYP/6-31+G* level using the Gaussian 03 program.[33] For the optimized complex, the transferred charges are then calculated by using the NBO version 3.1 module in Gaussian 03 at the same level, where natural population analysis and the second order perturbation theory analysis of the Fock matrix in the NBO basis are considered. The computations of force constants and the vibration frequencies indicate that after optimization the structure is a global minimum (Table S1, Supporting Information).

For zinc-finger protein, assuming a highly symmetric structure between zinc and ligands, Sakharov and Lim suggested that each ligand in the complex transfers the same amount of charge to the zinc. Thus, they calculated the amount of charge donated by each ligand simply from the partial charge on zinc.[23] Differently, the geometry of the $[Zn^{2+}(IMI)_3HCOO^-]^{1+}$ complex has lower symmetry. Thus, we have to explicitly calculate the charge donated from each ligating atom to zinc. On the basis of the values of second order perturbation energy in NBO calculation, the amount of charge accepted by zinc appears to be contributed mainly by the coordinating atoms. The π orbital metal-to-ligand donation can be excluded because the ligand atoms are all poor electron acceptors.[34] Therefore, here we focus on the charges donated by the atoms that directly bind to zinc. The transferred charge is then given by

$$\Delta q_{\mathrm{L}\to\mathrm{Zn}} = [F(\mathrm{L}, \mathrm{Zn})/(E_{\mathrm{Zn}} - E_{\mathrm{L}})]^2 \quad (2)$$

where $\Delta q_{\mathrm{L}\to\mathrm{Zn}}$ is the quantity of charge transferred from the lone pair orbital (LP) of the donated atoms to the anti-LP orbital (LP*) of zinc, F(L, Zn) presents the Fock matrix, and $E_{\mathrm{Zn}} - E_{\mathrm{L}}$ is the energy difference between LP* of zinc and LP of ligand atom L.

From the quantum calculation, the three ligating nitrogens in imidazoles and the ligating oxygen in carboxylate respectively donate 0.094e, 0.094e, 0.084e, and 0.13e, the sum of which occupies 98.5% of the amount of transferred charge, i.e., 0.41e, that zinc accepts. The equilibrium distances between zinc and the three ligating nitrogens and one oxygen are 2.05, 2.05, 2.08, and 1.98 Å, respectively. As implemented in the model by Sakharov and Lim,[23] the amount of charge $\Delta q_{\mathrm{L}\to\mathrm{Zn}}$ transferred from the ligand atom L to zinc is linearly related with their interatomic distance $r_{\mathrm{Zn,L}}$, as given by

dx.doi.org/10.1021/jp4021933 | J. Phys. Chem. B 2013, 117, 6138−6148

$$\Delta q_{L\rightarrow Zn} = a_L \times r_{Zn,L} + b_L \quad (3)$$

in which the atom L represents the ligating nitrogens in the imidazoles and the ligating oxygen in the formate. The charge transfer parameters, a_N and b_N, for nitrogens can be fixed if only two points on the line are given. Here, the first point is offered by the average equilibrium distance between ligating nitrogens and zinc $\overline{r}_{Zn,N} = (2.08 + 2.05 + 2.05)/3 = 2.06$ Å and the average transferred charge from ligating nitrogens to zinc $\overline{\Delta q}_{N\rightarrow Zn} = (0.094 + 0.094 + 0.084)/3 = 0.091$e. In order to make the charge transfer parameters consistent with the force field, the second point is obtained from the force field. The sum of the vdW radii of the ligating nitrogen and zinc is considered as the cutoff distance, at which the transferred charge reduces to zero. Thus, the charge of ligating atoms beyond the cutoff distance is constant. b_O and a_O for the ligating oxygen can be calculated in a similar fashion. At any time-step t during simulations, the transferred charge $\Delta q_{L\rightarrow Zn}$ is changed according to eq 3 only if $r_{Zn,L}$ is smaller than the sum of the vdW radii of zinc R_{Zn} and the ligating atoms.

In the paper, two sets of vdW parameters are discussed. As shown in Table 1, vdW2 is the vdW parameter set of zinc from the CHARMM22 force field,[35] which can reproduce the experimental first-shell Zn−O distances, coordinating numbers (CNs) in water, and the absolute experimental hydration free energies of zinc. vdW1 is the vdW parameter set of zinc obtained by adjusting vdW2 to reproduce the experimental hydration free energy of zinc relative to the hydration free energy of other metal dications.[36] Thus, two sets of a_L and b_L are determined, as given in Table 1.

Table 1. The Two Sets of vdW Parameters (vdW1 and vdW2) and the Corresponding Two Sets of Charge Transfer Parameters

	R_{Zn} (Å)	ε_{Zn} (kcal/mol)	a_N (e/Å)	b_N (e)	a_O (e/Å)	b_O (e)
vdW1	0.88	−0.183	−0.14	0.38	−0.22	0.57
vdW2	1.09	−0.25	−0.1	0.3	−0.16	0.45

2.2. Multiscale Point Dipole Model. In the model, we describe the dipoles with three scales, ranging from the residue-based level, to the backbone/side-chain-based level, and to the atom-based level. For the zinc binding site, if it is the backbone (or side chain) of a residue that binds to zinc, then the atom-based dipole is considered for the backbone (or side chain), and the polarization effect on the corresponding side chain (or backbone) is simulated with a single coarse-grained dipole. The residue-based dipoles are considered for all the residues that locate outside the zinc binding site. In detail, from the crystal structures obtained with NMR experiment, zinc tetrahedrally binds to the side chains of residues Glu11, His6, His13, and His14.[16] Thus, the dipoles are atom-based for the four coordinating side chains (see the red groups in Figure 1). Correspondingly, four backbone-based dipoles are applied to the backbones of these four residues (see the green balls in Figure 1). For the rest of the 12 amino acid residues, residue-based dipoles are defined (see the white balls in Figure 1).

The peptide atom−atom polarization interaction is much weaker compared with the polarization effect induced by zinc, and has been implicitly included in the CHARMM22 force field simply by adjusting atomic charges to reproduce the interaction energy.[35] Thus, in the present work, we follow the assumption by Sakharov and Lim[23] that the biomolecule is polarized utterly due to the electric field created by the charge of zinc. As a result, the polarization energy V^P is given by

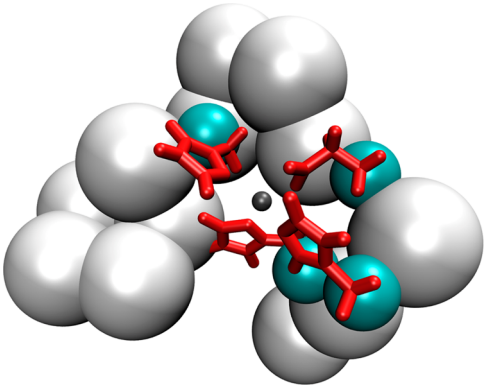

Figure 1. Schematic diagram of multiscale dipoles applied to the $A\beta_{1-16}$−Zn complex. Twelve big balls denote the residue-based dipoles. Four smaller balls represent the backbone-based dipoles. The chemical groups in bonds employ the atom-based dipoles. The small ball in the center is zinc.

$$V^P = V^A + (V^{PA}_{q,\mu} + V^{PA}_{\mu,\mu}) = -\frac{1}{2}\sum_i \vec{E}_i^{\,0}\cdot\vec{\mu}_i \quad (4)$$

where

$$V^A = \frac{1}{2}\sum_i (\vec{E}_i^{\,0} + \vec{E}_i^{\,\mu})\cdot\vec{\mu}_i \quad (5)$$

$$V^{PA}_{q,\mu} = -\sum_i \vec{E}_i^{\,0}\cdot\vec{\mu}_i \quad (6)$$

and

$$V^{PA}_{\mu,\mu} = -\frac{1}{2}\sum_i \vec{E}_i^{\,\mu}\cdot\vec{\mu}_i \quad (7)$$

in which the activation energy, V^A, is known as the self-polarization energy to create the induced dipoles of either peptide or zinc;[37] $V^{PA}_{q,\mu}$ denotes the total interaction energy between the point charge of zinc and induced dipoles of peptide and between the point charges of peptide atoms and the induced dipoles of zinc; and $V^{PA}_{\mu,\mu}$ denotes the total interaction energy between induced dipoles of peptide and induced dipoles of zinc. The sum of $V^{PA}_{q,\mu}$ and $V^{PA}_{\mu,\mu}$ is the polarization energy relative to V^A. Consequently, the net change in interaction energy, V^P, is obtained as in eq 4. The summations in eqs 4−7 are over all induced dipoles. $\vec{\mu}_i$ is the dipole moment of the ith induced dipole. $\vec{E}_i^{\,0}$ and $\vec{E}_i^{\,\mu}$ are the electric fields at site i and created by neighboring point charges and induced dipoles, respectively. Considering the electric fields at site i belonging to peptide, $\vec{E}_i^{\,0}$ is generated by the point charge of zinc and $\vec{E}_i^{\,\mu}$ by the induced dipole of zinc. For the electric fields at zinc, $\vec{E}_i^{\,0}$ is created by the point charges of all peptide atoms and $\vec{E}_i^{\,\mu}$ by the induced dipoles of peptide.

Assuming a linear response approximation, the induced dipole moment $\vec{\mu}_i$ at the ith site is proportional to the local electric field, $\vec{E}_i$ which is the sum of $\vec{E}_i^{\,0}$ and $\vec{E}_i^{\,\mu}$:

$$\vec{\mu}_i = \alpha_i\vec{E}_i \quad (8)$$

dx.doi.org/10.1021/jp4021933 | J. Phys. Chem. B 2013, 117, 6138−6148

where the proportionality constant α_i is the polarizability of the ith polarizable unit. In the current work, we assume that the polarizability is isotropic and constant. The standard polarizabilities of peptide residues and atoms can be found in the literature.[38,39] The polarizability of zinc is 2.294 Å^3.[40] The polarizability of the deprotonated nitrogen on an imidazole is 2.8 Å^3,[23] which is bigger than the value 1.09 Å^3 provided in earlier research.[39]

In fact, there are two factors that can affect the polarizabilities of polarizable atoms, namely, the amount of electrons and the distance of the electrons from nuclear charge. The polarizability of an atom increases as the amount or the distance increases, because the nuclear charge has less control on charge distribution. Electrons on a ligating side chain are delocalized and redistributed under strong electric field created by zinc. The redistribution of electrons leads to the increased polarizabilities of atoms that directly bind to zinc and the decreased polarizability of other atoms on the same side chain. Here, the polarizabilities of the ligating atoms are adjusted by multiplying the standard values with a parameter 2.8/1.09, while the atomic polarizabilities of other atoms on the same ligating side chain are modified simply by setting them to zero. As for the fragments out of the zinc binding site, we assume that the electric field created by zinc is able to distort the electron cloud of atoms but is not strong enough to affect the molecular orbital. Thus, the residual polarizability has to not be modified.

The total electric field $\vec{E}_{Zn}$ at zinc is the vector sum of the electric field due to the current charges of protein atoms and induced dipoles in protein:

$$\vec{E}_{Zn} = E^0_{Zn} + \sum_i T_{Zn,i}\vec{\mu}_i = \sum_j \frac{q_j \vec{r}_{Zn,j}}{r_{Zn,j}^3} + \sum_i \frac{\vec{\mu}_i}{r_{Zn,i}^3}\left(\frac{3\vec{r}_{Zn,i}\vec{r}_{Zn,i}}{r_{Zn,i}^2} - 1\right) \quad (9)$$

where $\vec{E}^0_{Zn}$ is the electric field created from the current charges of protein atoms with summation over all peptide atoms and $T_{Zn,i}$ is the ith element of the dipole field tensor with summation over all the induced dipoles in the peptide.

The total electric field $\vec{E}_i$ at the ith dipole in the peptide is the sum of the field $\vec{E}^0_i$ caused by the current charge and the field $T_{i,Zn}\vec{\mu}_i$ caused by the induced dipole on zinc:

$$\vec{E}_i = E^0_i + T_{i,Zn}\vec{\mu}_i = \frac{q_{Zn}\vec{r}_{i,Zn}}{r_{i,Zn}^3} + \frac{\vec{\mu}_{Zn}}{r_{i,Zn}^3}\left(\frac{3\vec{r}_{i,Zn}\vec{r}_{i,Zn}}{r_{i,Zn}^2} - 1\right) \quad (10)$$

In turn, the corresponding induced dipole moments are obtained with eq 8. Subsequently, we can solve the self-consistent field by iterating the coupled equations (i.e., eqs 8−10) until the convergence condition that the polarization energy change is smaller than a minimum (1.0^{-6} kcal/mol) is satisfied.

In order to avoid the calculation of the derivative of the polarization energy with respect to the induced dipole moments, the polarization energy is represented by another form here. Multiplying vector $\vec{\mu}_i$ on both sides of eq 10, we can obtain the following identity:

$$-\frac{1}{2}\sum_i \vec{\mu}_i\cdot\vec{E}^q_i - \frac{1}{2}\sum_i \vec{\mu}_i T_{i,Zn}\vec{\mu}_{Zn} + \frac{1}{2}\sum_i \vec{\mu}_i\cdot\alpha_i^{-1}\vec{\mu}_i = 0 \quad (11)$$

As a result, we rewrite the induced polarization energy in the following form:[41]

$$V^{pol} = -\sum_i \vec{\mu}_i\cdot\vec{E}^q_i - \frac{1}{2}\sum_i\sum_{j\neq i}\vec{\mu}_i T_{i,j}\vec{\mu}_j + \frac{1}{2}\sum_i \vec{\mu}_i\cdot\alpha_i^{-1}\vec{\mu}_i \quad (12)$$

Since the derivative with respect to any induced dipole moment is zero, the polarization forces can be derived as follows:

$$\vec{f}_{Zn} = (\vec{\mu}_{Zn}\cdot\nabla_{Zn})\vec{E}^q_{Zn} + \sum_i\left[(\vec{\mu}_i\cdot\nabla_{Zn})\vec{E}^q_i + \frac{1}{2}(\vec{\mu}_i\cdot\nabla_{Zn})T_{i,Zn}\vec{\mu}_{Zn} + \frac{1}{2}(\vec{\mu}_{Zn}\cdot\nabla_{Zn})T_{Zn,i}\vec{\mu}_i\right] \quad (13)$$

$$\vec{f}_i = (\vec{\mu}_i\cdot\nabla_i)\vec{E}^q_i + (\vec{\mu}_{Zn}\cdot\nabla_i)\vec{E}^q_{Zn} + \frac{1}{2}(\vec{\mu}_{Zn}\cdot\nabla_i)T_{Zn,i}\vec{\mu}_i + \frac{1}{2}(\vec{\mu}_i\cdot\nabla_i)T_{i,Zn}\vec{\mu}_{Zn} \quad (14)$$

The approximation used in eq 8 shows a growth of the induced dipoles with the distances between induced dipoles and zinc, which becomes no longer valid at close distances. In order to avoid unphysical growth of the induced dipoles at close distance, a cutoff distance $r^{cutoff}_{i,Zn}$ is considered, which is assumed to be equal to the sum of the vdW radii of atoms (residues) and zinc, and then multiplied by the parameter 0.92, as suggested in the literature.[23] For each dipole−dipole pair, $r_{i,Zn} = r^{cutoff}_{i,Zn}$ if $r_{i,Zn} \leq r^{cutoff}_{i,Zn}$.

The center of a coarse-grained dipole is the centroid of the corresponding molecular fragment (residue, backbone, or side chain in the peptide). Thus, the polarization force vector $\vec{F}_{pol}$ that goes through the dipole center does not cause rotating motion of the fragment. As a result, the polarization force $\vec{f}_{pol}$ acting on atoms that belongs to the fragment can be derived simply by the following equation

$$\vec{f}_i^{\,pol} = m_i\frac{\vec{F}^{pol}}{\sum_i m_i} \quad (15)$$

where m_i is the atomic mass with the summation over the atoms in the fragment.

2.3. Simulation Methodology. There are 20 conformers shown in the PDB file of $A\beta_{1-16}$−Zn (PDB ID: 1ZE9), and the first one is suggested to be the best representative of the ensemble, which is the one that best satisfies all of the constraints (i.e., distance and dihedral angle constraints).[16] As a fact, the differences between these 20 conformers are pretty small, because the calculated root-mean-square displacement of them is only 0.89 Å. Thus, in this work, the first conformer is chosen as the starting structure of the simulations. As to the atom−atom interaction between peptide atoms, we employ the popular all-atom CHARMM22 force field in conjunction with the two-dimensional (2D) dihedral energy correction map (CMAP) extension.[35,42] CHARMM22 is parametrized in reproducing protein conformational distributions in MD simulations. CMAP is a 2D dihedral energy correction map to the CHARMM22 and used to improve the sampling of backbone torsion angles. Here, the CHARMM22/CMAP is

dx.doi.org/10.1021/jp4021933 | J. Phys. Chem. B 2013, 117, 6138−6148

called the traditional force field. The MD simulations in either explicit or implicit solvent have been carried out in NVT ensembles under an experimental temperature of 278 K. All simulations are carried out near neutral pH, so the acid residues such as Glu and Asp are deprotonated, whereas base residues like Arg and Lys are protonated.

Explicit solvent MD simulations with standard software are performed under the traditional force field. On the other hand, implicit solvent MD simulations are performed under the new force field where charge transfer and induced polarization effect are added to the traditional force field.

2.3.1. Explicit Solvent Simulations. The MD simulation software NAMD is used to simulate the $A\beta_{1-16}$–Zn complex solvated in a water box filled with TIP3P water molecules.[43] Counterions are not needed for the neutral $A\beta_{1-16}$–Zn complex. The vdW and electrostatic forces are switched at a distance of 10.0 Å to zero at 12.0 Å. A Langevin thermostat is used to keep the temperature constant, and the viscosity is 10 ps^{-1}.[44,45] The time step is 1 fs. In order to eliminate close contacts, first the solute $A\beta_{1-16}$–Zn is fixed, while the solvent is relaxed at an NVE ensemble until the water reaches equilibrium. Second, the solute is released, and the whole system undergoes 50 ps of energy minimization. Finally, a 30 ns simulation is carried out.

2.3.2. Implicit Solvent Simulations. Simulations with explicit solvent molecules require prohibitive costs of computer resource and time especially in solvent relaxing. Implicit solvent has been proved to be more efficient than explicit solvent for a small peptide complex like $A\beta_{1-16}$–Zn. Thus, in order to speed up the simulation and meanwhile to improve the efficiency of sampling with a short simulation, we employ the generalized Born/solvent accessible surface area (GB/SASA) model[46−48] as an implicit solvent model. The GB method approximates the polar contribution to the solvation free energy, while the nonpolar contribution can be approximated with a term proportional to the SASA.[49]

The GB model adopted here is originally proposed by Still and co-workers[50] and parametrized later specifically for proteins, peptides, and nucleic acids within the CHARMM all hydrogen and polar hydrogen force fields.[46] Compared with the standard numerical values derived from the finite differential Poisson−Boltzmann (FDPB) method implemented in the software Delphi,[51] the vdW radius of zinc as the intrinsic radius in the GB model would produce an underestimated effective Born radius of zinc and therefore overestimated solvation free energy. In order to overcome these problems, following the approach applied to the intrinsic radius of polar hydrogen,[46,50,52] we set the intrinsic radius of zinc to 1.8 Å.

SASA values are obtained with the LCPO approximation[47] with a solvent probe radius of 1.4 Å. Atomic SASAs are computed by using

$$A_i = P_1 S_1 + P_2 \sum_{j\in N(i)} A_{ij} + P_3 \sum_{\substack{j,k\in N(i)\\ k\in N(j)\\ k\neq j}} A_{jk} + P_4 \sum_{j\in N(i)} A_{ij} \left(\sum_{\substack{j,k\in N[i)\\ k\in N(j)\\ k\neq j}} A_{jk} \right) \quad (16)$$

where $N(i)$ denotes the neighbor list (NL) of i (the list of neighboring spheres that overlap with sphere i). In the first term, S_1 is the surface area of the isolated sphere corresponding to atom i. A_{ij} is the area of sphere i buried inside sphere j. Therefore, the second term involves the sum of pairwise overlaps of sphere i with its neighbors. The third term presents the sum of overlaps of neighbors of i with each other. The fourth term is a further correction for multiple overlaps. Besides, in order to further improve computational efficiency, an optimization method called neighbor-list reduction (NLR)[48] is employed when SASA is computed, which allows selected neighbors of a central atom to be removed from the computation in a preprocessing step. Thus, it allows the calculation of the atom's surface area to proceed with a shorter list of neighbors.[48] In the current work, new parameters P_1 to P_4 with respect to different types of atoms for both LCPO and LCPO/NLR are derived using our own training set of zinc proteins so as to make them consistent with the CHARMM22 force field (Table S2, Supporting Information). Given the total SASA of the solute, the nonpolar solvation free energy is equal to SASA timing a phenomenological surface tension coefficient of 0.00542 kcal/(mol·$Å^2$).

The implicit solvent simulations are also combined with Langevin dynamics with the same viscosity, 10 ps^{-1}. Notably, the external friction and random forces here act only on the heavy atoms on the peptide surface to avoid unphysical fluctuations of buried atoms. The time step is set at 1 fs too, but the cutoff approach is not used. Similarly, in order to avoid close contacts, the energy of the complex is minimized for 50 ps before a 15 ns simulation is carried out.

3. RESULTS

Mainly two MD simulations of the $A\beta_{1-16}$–Zn complex solvated in the implicit solvent are carried out in the current work. The first simulation (Sim1) adopts the model proposed by Sakharov and Lim,[23] where only the atom-united dipoles are considered for the side chains that directly bind to zinc with the vdW parameter set of vdW1 (see Table 1). The second simulation (Sim2) corresponds to our model, in which the multiscale dipoles are used to account for the polarization effect of zinc on the whole peptide. Sim2 adopts the vdW parameter set of vdW2 (see Table 1). In order to compare the results produced by Sim1 and Sim2, some structural and dynamic quantities are computed by averaging along the trajectories. Images are rendered with VMD.[53]

3.1. Root-Mean-Square Deviation (RMSD). In the simulation, the initial positions of atoms are determined from the NMR structure. Because in the NMR structure the first and the last residues are weakly defined, the RMSD of the backbone Ca atoms is then calculated without these two residues. The RMSD trajectory for $A\beta_{1-16}$ is given by the blue solid line in Figure 2. The RMSD trajectory of the backbone Ca atoms for the minimal zinc binding domain, $A\beta_{6-14}$, including all four coordinating a.a. residues, is also plotted with a green dashed line in Figure 2. The RMSD trajectory of a zinc binding center, containing zinc and another five atoms that directly bind to it, is shown by the red dotted line in Figure 2.

For Sim1 in Figure 2a, the RMSD of $A\beta_{6-14}$ equilibrates fast and keeps stable throughout the simulation, but there are two evident jumps away from the native structure for the RMSDs of $A\beta_{1-16}$ and the zinc binding center before they reach equilibrium. Differently, one can see that all three RMSD

dx.doi.org/10.1021/jp4021933 | J. Phys. Chem. B 2013, 117, 6138−6148

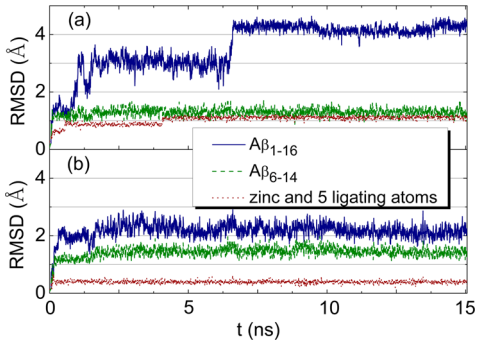

Figure 2. RMSD trajectories as a function of time derived from (a) Sim1 and (b) Sim2. The RMSDs of the backbone Ca atoms for the whole peptide $A\beta_{1-16}$ and for minimal zinc binding domain $A\beta_{6-14}$ are represented with solid lines and dashed lines, respectively. The RMSD of the zinc binding center, including zinc and another five atoms that directly bind to zinc, is plotted with dotted lines.

trajectories keep stable after the short transient period for Sim2 in Figure 2b.

Averaging the RMSD trajectories along the time after convergence (here and after we use the period of the last 5 ns as the sampling region), the mean as well as standard deviation of RMSD is obtained (Table S3, Supporting Information). One can see that either Sim1 or Sim2 is able to retain the structure of the minimal zinc binding domain (1.30 Å for Sim1 and 1.44 Å for Sim2); however, Sim2 produces much smaller RMSD values of whole $A\beta_{1-16}$ and RMSD values of the zinc binding center. The smaller RMSD of $A\beta_{1-16}$ for Sim2 indicates the significance of the induction effect of zinc on the structural stabilization of the global region of $A\beta_{1-16}$ peptide. Thus, compared to Sim1, Sim2 replicates better the conformational stabilization of the N-terminal region in the presence of zinc. The use of vdW2 as well as the rescaling of atomic polarizability to the atoms on ligating side chains can stabilize better the structure of the zinc binding center.

3.2. Radius of Gyration. Now we discuss the radius of gyration R_g which is defined as

$$R_g = \sqrt{\frac{m_i(\vec{r_i} - \vec{r_c})^2}{\sum_i^N m_i}} \quad (17)$$

where $\vec{r_c}$ is the vector to specify the center of mass of the complex with N atoms, $\vec{r_i}$ is the position vector of atom i with mass m_i, and the sum is over the N atoms in the complex. The radius of gyration as a function of time is illustrated in Figure 3, where the blue dashed line is the R_g^0 of the NMR structure.

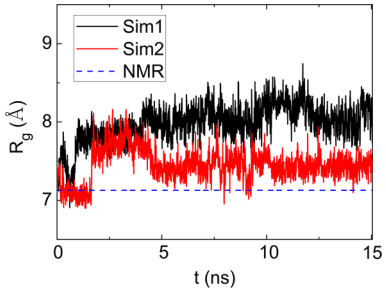

Figure 3. Trajectories of the radius of gyration of the complex $A\beta_{1-16}$–Zn as a function of time given by Sim1 and Sim2. The dashed line is the standard value derived from the NMR structure.

Compared with R_g^0, Sim2 provides a better R_g than Sim1. It has been stressed in the literature that the structure of $A\beta_{1-16}$ would become more compact upon zinc binding.[16] Thus, the bigger R_g^0 with higher fluctuations produced by Sim1 is similar to that found in apo $A\beta_{1-16}$, implying that the impact of zinc is underestimated in Sim1. These results indicate that the global consideration of the zinc-induced dipoles is critical to keep the complex under a reasonable radius of gyration.

3.3. Coordination Geometry and Secondary Structure. In the NMR structure, zinc is tetrahedrally coordinated to four a.a. residues, namely, Glu11 and His(6, 13, and 14). The carboxylate side chain of Glu11 binds to zinc in a bidentate fashion with the Zn–O distance 2.11 Å. *Nδ* atoms of His6 and His14 have a distance of about 2.1 and 2.3 Å from zinc, respectively, while the *Nε* atom of His13, about 2.14 Å.

With Sim2, two oxygens on the carboxylate coordinate with zinc, as highlighted in Figure 4b. However, with Sim1, one of

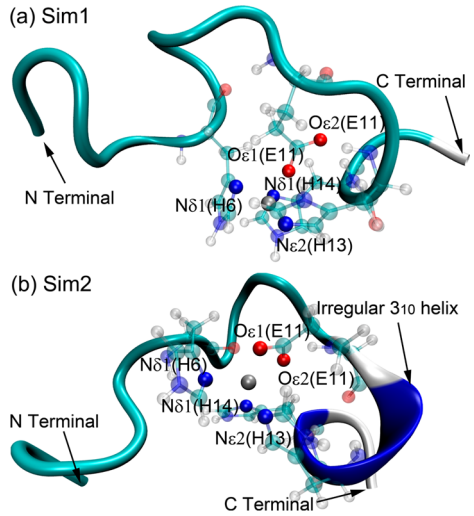

Figure 4. Snapshots of the $A\beta_{1-16}$–Zn complex obtained from MD simulations (a) Sim1 and (b) Sim2, respectively. The ligating residues (His(6, 13, and 14) and Glu11) are illustrated with ball-bond mode. The coordinating atoms, including *Nδ*1 (His6), *Nε*2 (His13), *Nδ*1 (His14), *Oε*1 (Glu11), and *Oε*2 (Glu11), are highlighted by making the rest of the atoms transparent. The abbreviations E and H denote Glu and His, respectively. The helix-like structure is the irregular 3_{10} helix.

the two ligating oxygens is excluded off the zinc binding center (Figure 4a). As far as we know, we are the first to capture the bidentate mode of Glu11 bound to zinc in the $A\beta_{1-16}$–Zn complex with MD simulation based on the model without any bond or angle constraint. In fact, from the optimized structure of the complex $[Zn^{2+}(IMI)_3HCOO^-]^{1+}$, the carboxylate forms asymmetrical ZN–O bonds with zinc (1.98 and 2.48 Å), which is consistent with the results derived from the previous QM studies.[28,54] It has been suggested that the bidentate binding fashion characterized by weaker Zn–O bond strength and similar Zn–O bond length observed in proteins depends not only on the Zn–O interactions but also on other interactions among ligands[55] under a certain protein environment. We found that *Oε*1 (Glu11) is involved in two hydrogen bonds with *Hβ*2–*Cβ* (His14) and H–N (Glu11), respectively, while *Oε*2 (Glu11) keeps a strong interaction with *Hε*1 (HIS13) (data not shown). These extra interactions are in agreement

dx.doi.org/10.1021/jp4021933 | J. Phys. Chem. B 2013, 117, 6138–6148

with the NMR structure. As a consequence, our method can capture the bidentate binding mode.

Differently, the use of a smaller radius of zinc in Sim1 directly leads to the exclusion of $O\varepsilon1$ (Glu11) due to the limit in the space of the zinc binding center. From Table 2, one can see that, compared to the NMR data, Sim2 gives better coordination bond lengths than Sim1. The mean absolute deviation of the bond lengths from the NMR data obtained by Sim2 is 0.056 Å, which is much smaller than 0.51 Å obtained by Sim1.

Table 2. The Comparison of Coordination Bond Length Obtained by Sim1, Sim2, and NMR

coordination bond length (Å)	Sim1	Sim2	NMR
$N\delta$ (His6)	1.96 ± 0.04	2.14 ± 0.04	2.10 ± 0.01
$N\varepsilon$ (His13)	1.92 ± 0.04	2.16 ± 0.04	2.14 ± 0.01
$N\delta$ (His14)	1.93 ± 0.04	2.14 ± 0.04	2.29 ± 0.02
$O\varepsilon_1$ (Glu11)	1.92 ± 0.06	2.06 ± 0.04	2.10 ± 0.01
$O\varepsilon_2$ (Glu11)	3.83 ± 0.09	2.07 ± 0.04	2.11 ± 0.01

There is an irregular 3_{10} helix in the C terminus of $A\beta_{1-16}$ characterized by two hydrogen bonds formed by backbone O (Glu11)−H−N (His14) (HBond1) and O (Val12)−H−N (Gln15) (HBond2), respectively. When the distance between donor (backbone O) and acceptor (backbone N) is smaller than 3.5 Å and simultaneously the hydrogen bond angle is bigger than 110°, a hydrogen bond is considered to exist. The mean distances as well as angles of the two backbone hydrogen bonds are listed in Table 3. These results indicate that, although the HBond2 is captured, Sim1 fails in reproducing the HBond1, since the donor−acceptor distance 4.46 Å exceeds the up limit.

From Table 3, one can see that both HBond1 and HBond2 are kept by Sim2. Thus, the irregular 3_{10} helix can be observed in Sim2 (see Figure 4b), which is consistent with the experimental observation.

3.4. Solvent Exposure of Residues. Here, the solvent exposure of a residue (SE-Res) is specified by the solvent accessible surface area of the residue. As illustrated in Figure 5, except for the residue Glu3, to which either Sim1 or Sim2 provides overestimated SE-Res, Sim2 in general shows a better tendency of SE-Res over the a.a. residue sequence, because the mean absolute/relative error of SE-Res over the 17 residues is 33.7/0.40 Å^2 for Sim1 and 22.8/0.29 Å^2 for Sim2. Notably, in order to capture the global error, the individual big relative errors for residue 14 (i.e., 21.7 Å^2 for Sim1 and 7.7 Å^2 for Sim2) are not counted in.

Here, both Sim1 and Sim2 retain the four buried coordinating residues (His(6, 13, and 14) and Glu11) due to the existence of zinc. However, compared with the experimental data, the estimated values of SE-Res of Glu11 and His14 with Sim1 are worse than those with Sim2. It has been noted that, in contrast to the locations of residues Phe4 and Tyr10 in the apo $A\beta_{1-16}$ monomer (PDB ID: 1ZE7), residue Phe4 is located in the inner core of the structures and Tyr10 is excluded from the coordination sphere and systematically locates on the surface opposed to the zinc ion.[16] As highlighted in Figure 5, the results for Tyr10 and Phe4 are plotted with solid squares for Sim1 and solid circles for Sim2. On the other hand, Sim1 overestimates the SE-Res of Phe4, making this nonpolar residue, like in apo $A\beta_{1-16}$, stay on the surface of the peptide.[16] On the other hand, for Sim2 in which the polarization effect has been considered for the whole domain, the SE-Res of Phe4 is consistent with the experimental data. Meanwhile, the solvent exposures of another three nonpolar residues (Ala2, Glu9, and Val12) provided by Sim2 are in good agreement with the experimental observation, as shown in Figure 5.

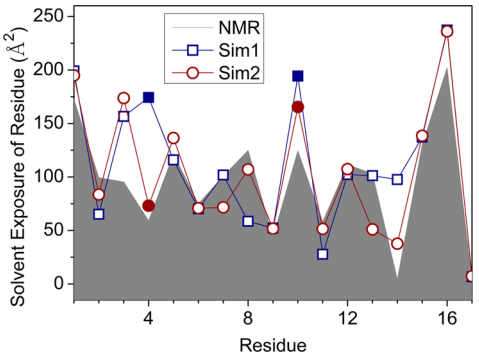

Figure 5. Solvent exposure of 17 residues in the $A\beta_{1-16}$−Zn complex provided by Sim1 (open squares) and Sim2 (open circles). Zinc is the 17th residue. The corner points of the shadow represent the solvent exposure of residues derived from the NMR structure. The results for residues Tyr10 and Phe4 are highlighted with solid squares for Sim1 and solid circles for Sim2.

The disagreement of SE_Res for residues Glu3 and Tyr10 could be explained as follows. First, among 20 NMR conformers of $A\beta_{1-16}$−Zn (PDB ID: 1ZE9), residues Glu3 and Lys16 stay close to each other in some conformers, including the first conformer, whereas in other conformers they are separated. In both Sim1 and Sim2, residues Glu3 and Lys16 remaining apart are observed, giving the disagreement of SE_Res for residue Glu3. Also, the separation is probably due to the screening effect of implicit solvent on the electrostatic interaction between residue side chains on the peptide surface. Second, as to the residue Tyr10 that also locates on the surface of peptide, the weakened electrostatic interactions and the resulting decoupling with some other residues are likely due to the screening effect of implicit solvent too.

3.5. Ligand Exchange. There is not any explicit water molecule involved in the implicit solvent simulations, so it is difficult to judge whether our model (Sim2) is able to capture the experimentally observed tetrahedral coordination mode once explicit water molecules are presented. We found that at

Table 3. The Comparison of Hydrogen Bond Angles and Donor−Acceptor Distances in Hydrogen Bonds Obtained by NMR, Sim1, and Sim2

	hydrogen bond angle (deg)		donor−acceptor distance (Å)	
	HBond1	HBond2	HBond1	HBond2
NMR	148.98 ± 3.65	153.30 ± 9.95	3.32 ± 0.09	3.03 ± 0.12
Sim1	146.75 ± 9.17	119.81 ± 20.06	4.46 ± 0.27	3.43 ± 0.63
Sim2	135.86 ± 13.18	122.68 ± 15.48	3.00 ± 0.17	3.46 ± 0.25

dx.doi.org/10.1021/jp4021933 | J. Phys. Chem. B 2013, 117, 6138−6148

least it is negative for the explicit solvent simulation with the traditional force field using vdW2, because zinc is found to be hexacoordinated with the four residues mentioned above and another two water molecules.

Consequently, we design a simple hybrid solvent model that the bulk solvent is implicitly presented with the two coordinating water molecules explicitly described. Here, the explicit water molecules are modeled with the TIP3P model and the force field parameters come from CHARMM22.[35] The starting structure is the equilibrium structure derived from an explicit solvent simulation with the traditional force field, in which vdW2 is used. Note that in the starting structure the carboxylate of Glu11 monodentately binds to zinc. Following the scheme suggested by Sakharov and Lim,[23] the induced polarization effect and the charge transfer effect on water molecules are ignored in the current implement. The total simulation time is 1000 ps for the study of ligand exchange. It is found that there is not any ligand exchange happening after 1 ps; thus, only the time area from 0 to 1 ps in which ligand exchange occurs is displayed in Figure 6c.

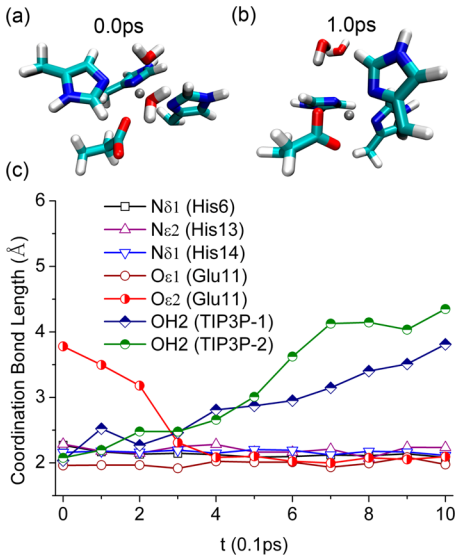

Figure 6. Coordination bond length varying as a function of time. Snapshots of $A\beta_{1-16}$–Zn at the time points 0.0 ps (a) and 1.0 ps (b) are extracted from the MD simulation in the hybrid solvent. For $A\beta_{1-16}$, only the coordinating side chains are displayed and the solid ball in the center is zinc. Coordination bond length of seven atoms with zinc are calculated (c), including $N\delta1$ (His6) given by open squares, $N\varepsilon2$ (His13) by up triangles, $N\delta1$ (His14) by down triangles, $O\varepsilon1$ (Glu11) by open circles, $O\varepsilon2$ (Glu11) by red half-open circles, $OH2$ (TIP3P-1) by blue half-open diamonds, and $OH2$ (TIP3P-2) by green half-open circles, respectively.

The coordination bond lengths for seven atoms, including $N\delta1$ (His6), $N\varepsilon2$ (His13), $N\delta1$ (His14), $O\varepsilon1$ (Glu11), $O\varepsilon2$ (Glu11), $OH2$ (TIP3P-1), and $OH2$ (TIP3P-2), are presented in Figure 6c as a function of time. The results show that at the beginning the bond lengths concerned with the oxygens on the two explicit water molecules increase and simultaneously the bond length of $O\varepsilon2$ (Glu11)–Zn reduces. The exchange process ends at 0.4 ps, and from then on, the new $O\varepsilon2$ (Glu11)–Zn bond maintains. Zinc-induced polarization force enables coordinating atoms, $N\delta1$ (His6), $N\varepsilon2$ (His13), $N\delta1$ (His14), $O\varepsilon1$ (Glu11), and $O\varepsilon2$ (Glu11), to remain bound to the metal. Therefore, it is not expected to see ligand exchange again. The conformations of the zinc binding site at 0.0 and 1.0 ps are displayed in parts a and b of Figure 6, respectively, from which one can see that two water molecules are replaced by one of the O atoms of the Glu11. As for another four atoms not involved in ligand exchange, their bond lengths on average show nearly no change all through the simulation, implying that an individual coordinating bond length is predominated by the vdW radius of zinc. As a result, vdW2 is essential to obtain a satisfied coordinating bond length for the $A\beta_{1-16}$–Zn complex. We also find that, if the traditional force field is used, there is not any exchange of ligands observed, which demonstrates that implicit solvent does not influence the coordinating configuration generated in explicit solvent.

3.6. MD Simulation of Rat $A\beta_{1-16}$ Dimer Complexed with Zinc. The NMR solution structure of rat $A\beta_{1-16}$ dimer upon zinc binding (rat $2A\beta_{1-16}$–Zn) (PDB ID: 2LI9) is determined recently to explore the mechanism of rats' resistance to pathogentic $A\beta$ aggregation in AD.[56] The NMR measurements of this complex were carried out also at 278 K. In the rat $2A\beta_{1-16}$–Zn complex, zinc is tetrahedrally coordinated with four histidines. Both rat $A\beta_{1-16}$ monomers contribute two histidines (His6 and His14). Obviously, the zinc binding sites are catalytic. The charge transfer parameters listed in Table 1 are employed also for the system. According to the scheme of multiscale dipoles, the side chains of the four histidines use atom-based dipoles, the corresponding four backbone segments adopt backbone-based dipoles, and the other 28 residues employ residue-based dipoles. Similarly, we carry out another two simulations for 4 ns with respect to this system. One simulation (rSim1) follows the scheme by Sakharov and Lim,[23] and the other (rSim2) uses our model.

The RMSDs of the backbone Ca atoms for the whole dimer (rat $2A\beta_{1-16}$) and for the zinc binding domain (rat $2A\beta_{6-15}$) are calculated as a function of time. With respect to the rat $2A\beta_{1-16}$, the first and last residues of the peptide are discarded in the calculation of RMSD. From the RMSD trajectories, as shown in Figure 7, one can see that, for both rat $2A\beta_{6-15}$ and $2A\beta_{1-16}$, rSim2 provides a smaller RMSD than that obtained by rSim1, indicating that our model is also applicable to rat $2A\beta_{1-16}$.

4. DISCUSSION

It has been shown that most traditional force fields share a common limit in the calculation of electrostatic potential due to a lack of treatment of the electronic polarization effect. Currently, the point dipole model is one of the most widely

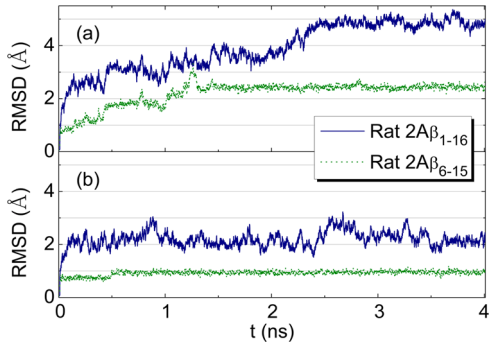

Figure 7. RMSD trajectories as a function of time derived from (a) rSim1 and (b) rSim2. The RMSDs of the backbone Ca atoms for the whole dimer (rat $2A\beta_{1-16}$) and for the zinc binding domain (rat $2A\beta_{6-15}$) are represented with solid lines and dotted lines, respectively.

dx.doi.org/10.1021/jp4021933 | J. Phys. Chem. B 2013, 117, 6138–6148

used polarizable models, but this model requires a large amount of calculations as the number of induced dipoles increases, hindering its extensive application to large systems. In this paper, we incorporate induced dipoles with multiscale modeling into all-atom simulations of $A\beta_{1-16}$–Zn to explicitly consider the polarization effect of zinc on $A\beta_{1-16}$. Our model (Sim2) can be applied not only to $A\beta_{1-16}$–Zn but also to other zinc proteins with similar zinc binding sites. In addition, based on quantum chemistry calculation, the charge transfer effect is empirically included in the simulations.

As a comparison, another model (Sim1) which exactly follows Sakharov and Lim's method[23] is also discussed. From the results, we show that, although the model Sim1 is appropriate for the proteins with structural-type zinc binding sites,[23] it is subjected to three deficiencies in describing $A\beta_{1-16}$–Zn structure: (1) The N terminus of $A\beta_{1-16}$ is not well stabilized and the irregular 3_{10} helix in the C terminus of $A\beta_{1-16}$ is not found. (2) The zinc binding site is overcompact, and Glu11 prefers monodentate binding to zinc. (3) Phe4 locates on the surface of $A\beta_{1-16}$. Nevertheless, all three deficiencies have been nicely solved with our model Sim2.

From the RMSD results of the zinc binding center, we show that, combined with proper vdW parameters, induced polarization of zinc is essential for reproducing the first-shell coordination geometry evaluated by NMR experiment. First, Sim2 uses vdW2, in which the radius of zinc is bigger than the one in vdW1 adopted by Sim1. Such a bigger radius of zinc directly loosens the zinc binding site, making room for the bidendate coordination of Glu11. Second, zinc-induced rearrangement of electrons on the coordinating side chains is of importance and should be taken into account. Taking His13 as an example, from the QM computation, we find that even though zinc accepts charge from the coordinating atom $N\varepsilon2$, the net charge on $N\varepsilon2$ still increases, rather than reduces. The increasing part is contributed by the rest of the atoms of the imidazole ring. In a previous study, as zinc got close to the side chain of His, the induced polarization of the whole imidzaole was presented by increasing the charge of the coordinating atom $N\varepsilon2$ with the decreasing charge on the rest of the atoms in the imidazole ring.[24] The model Sim1 modifies only the polarizability of the ligating atoms that directly bind to zinc. In the current paper, we reset the atomic polarizabilities on the ligating side chains to present the electron-delocalization effect, such as the increased polarizability of the coordinating atom $N\varepsilon2$ and the reduced polarizability of the rest of the atoms in the imidazole ring.

For zinc proteins with structural-type zinc binding centers, e.g., zinc-finger protein, a significant amount of charge (≈0.7e)[23] is transferred from coordinating atoms to zinc, leading to an obvious reduction of charge on zinc and subsequently weakening the polarization capacity of zinc. Therefore, it is unnecessary to globally consider the induction effects of zinc on the proteins. However, regarding the $A\beta_{1-16}$–Zn peptide with a catalytic-type zinc binding center, we suggest that the polarization force induced by zinc in the domains outside the zinc binding site should also be taken into account so as to stabilize the N-terminal region of $A\beta_{1-16}$ which is disordered in apo $A\beta_{1-16}$.[16] This is because the charge transfer effect plays less important roles in the interaction between $A\beta_{1-16}$ and zinc, due to less charge (≈0.4e) being transferred from coordinating atoms to zinc. As a result, the polarization effect of zinc out of the zinc binding site should not be ignored for $A\beta_{1-16}$–Zn.

It has been suggested that one of the possible zinc-induced aggregating mechanisms is that zinc induces the conformational change of $A\beta$ to facilitate aggregation.[8,26] For example, zinc induces exposing of hydrophobic groups, which promotes $A\beta$ aggregation in aqueous solvent. One possible interpretation for the location of Phe4 in the core of the peptide is that Phe4 is involved in hydrophobic interactions with other nonpolar groups. However, there are only four nonpolar residues (Ala2, Phe4, Glu9, and Val12) in $A\beta_{1-16}$ peptide and no hydrophobic core composed by them is found in either apo $A\beta_{1-16}$ or $A\beta_{1-16}$–Zn.[16] Noting that Phe4 is equally polarizable as polar residues, we suggest that the zinc-induced dipole on Phe4 forms a considerably attractive interaction with zinc, determining the Phe4 to stay in the core of the peptide. As a result, the location of Phe4 is modulated mainly by zinc through the induced polarization force.

In order to demonstrate the ability of our model to reproduce the tetrahedral coordination mode in the presence of explicit water molecules, we have carried out an additional MD simulation with a hybrid solvent. Our simulation result echoes the conclusion by Sakharov and Lim that the induced polarization effect combined with charge transfer effect is critical in avoiding unwanted water bound to zinc.[23] Charge transfer reduces the magnitudes of partial charge on zinc and therefore attenuates the electrostatic interaction between zinc and surrounding atoms. However, the zinc-induced polarization force on the O atom of the Glu11 compensates for the loss, enabling the O atom on this residue to substitute the two water molecules as a ligating atom.

We conclude that, to model the $A\beta_{1-16}$–Zn complex involved in Alzheimer's disease, (1) R_{Zn} = 1.09 Å is more appropriate as the radius of zinc in the framework of the CHARMM22 force field in studying catalytic-type zinc binding sites, and (2) most important of all, the polarization effect of zinc should be extended to the domains beyond the zinc binding site for $A\beta_{1-16}$-like peptide. From the simulations of rat $A\beta_{1-16}$ dimer upon zinc binding, we show that our model can be applied to other $A\beta_{1-16}$–Zn-like complexes.

■ ASSOCIATED CONTENT

Supporting Information

The results of force calculations to demonstrate that the optimized structure of $[Zn^{2+}(IMI)_3HCOO^-]^{1+}$ is a global minimum are given. LCPO and LCPO/NLR parameters inline with the CHARMM22 force field are also given. In addition, the mean and standard deviation of RMSD derived from Sim1 and Sim2 are given. In the end, two references with complete author lists are given. This material is available free of charge via the Internet at http://pubs.acs.org.

■ AUTHOR INFORMATION

Corresponding Author

*E-mail: jianweishuai@xmu.edu.cn. Phone: (86) 592-218-2575. Fax: (86) 592-218-9426.

Notes

The authors declare no competing financial interest.

■ ACKNOWLEDGMENTS

We thank Prof. Wen-Fei Li and Prof. Ye Mei for their helpful comments. We also thank Prof. Lin-Xiang Zhou and Prof. Xin-Li Liao for their warm help with the use of software NAMD and Gaussian. Helpful information offered by Prof. Dmitri V.

Sakharov and Prof. Carmay Lim is appreciated. We acknowledge support from the National Natural Science Foundation of China under grant 30970970, the China National Funds for Distinguished Young Scientists under grant 11125419, and the Funds for the Leading Talents of Fujian Province. Computational support from the Key Laboratory for Chemical Biology of Fujian Province, Xiamen University, and Xiamen Super Computing Center is gratefully acknowledged.

REFERENCES

(1) Goedert, M.; Splillantini, M. G. A Century of Alzheimer's Disease. *Science* **2006**, *314*, 777−781.
(2) Bush, A. I. The Metallobiology of Alzheimer's *Disease*. *Trends Neurosci.* **2003**, *26*, 207−214.
(3) Cuajungco, M. P.; Faget, K. Y. Zinc Takes the Center Stage: Its Paradoxical Role in Alzheimer's Disease. *Brain. Res. Rev.* **2003**, *41*, 44−56.
(4) Maynard, C. J.; Bush, A. I.; Masters, C. L.; Cappai, R.; Li, Q. X. Metals and Amyloid-β in Alzheimer's Disease. *Int. J. Exp. Pathol.* **2005**, *86*, 147−159.
(5) Tsvetkov, P. O.; Popov, I. A.; Nikolaev, E. N.; Archakov, A. I.; Makarov, A. A.; Kozin, S. A. Isomerization of the Asp7 Residue Results in Zinc-Induced Oligomerization of Alzheimer's Disease Amyloid-β (1−16) Peptide. *ChemBioChem* **2008**, *9*, 1564−1567.
(6) Sahoo, K. G. B.; Kaushalya, S. K.; Desai, R.; Maiti, S. Zinc Lowers Amyloid-β Toxicity by Selectively Precipitating Aggregation Intermediates. *Biochemistry* **2007**, *46*, 10655−10663.
(7) Duce, J. A.; Bush, A. I. Biological Metals and Alzheimer's Disease: Implications for Therapeutics and Diagnostics. *Prog. Neurobiol.* **2010**, *92*, 1−18.
(8) Ghaleh, N. R.; Giller, K.; Becker, S.; Zweckstetter, M. Effect of Zinc Binding on β-Amyloid Structure and Dynamics: Implications for *A*β Aggregation. *Biophys. J.* **2011**, *101*, 1202−1211.
(9) Chen, W. T.; Liao, Y. H.; Yu, H. M.; Cheng, I. H.; Chen, Y. R. Distinct Effects of Zn2+, Cu2+, Fe3+, and Al3+ on Amyloid-β Stability, Oligomerization, and Aggregation. *J. Biol. Chem.* **2011**, *286*, 9646−9656.
(10) Tougu, V.; Palumaa, P. Coordination of Zinc Ions to the Key Proteins of Neurodegenerative Disease: *A*β, APP, α-Synuclein and PrP. *Coord. Chem. Rev.* **2012**, *256*, 2219−2224.
(11) Furlan, S.; Penna, G. L. Modeling of the Zn Binding in the 1−16 Region of the Amyloid-β Peptide Involved in Alzheimer's Disease. *Phys. Chem. Chem. Phys.* **2009**, *11*, 6468−6481.
(12) Tsvetkov, P. O.; Kulikova, A. A.; Golovin, A. V.; Tkachev, Y. V.; Archakov, A. I.; Kozin, S. A.; Makarov, A. A. Minimal Zn Binding Site of Amyloid-β. *Biophys. J.* **2010**, *99*, 84−86.
(13) Fezoui, Y.; Teplow, D. B. Kinetic Studies of Amyloid β-Protein Fibril Assembly. *J. Biol. Chem.* **2002**, *277*, 36948−36954.
(14) Chen, Y. R.; Huang, H. B.; Chyan, C. L. The Effect of *A*β Conformation on the Metal Affinity and Aggregation Mechanism Studied by Circular Dichroism Spectroscopy. *J. Biochem.* **2006**, *139*, 733−740.
(15) Anand, P. F.; Nandel, S.; Hansmann, U. H. E. The Alzheimer's Beta Amyloid (*A*β 1−39) Monomer in an Implicit Solvent. *J. Chem. Phys.* **2008**, *128*, 165102.
(16) Zirah, S.; Kozin, S. A.; Mazur, A. K.; Blond, A.; Cheminant, M.; Milazzo, I. S.; Debey, P.; Rebuffat, S. Structural Changes of Region 1−16 of the Alzheimer Disease Amyloid-β Peptide upon Zinc Binding and in Vitro Aging. *J. Biol. Chem.* **2006**, *281*, 2151−2161.
(17) Stote, R. H.; Karplus, M. Zinc Binding in Proteins and Solution: A Simple but Accurate Nonbonded Representation. *Proteins* **1995**, *23*, 12−31.
(18) Bredenberg, J.; Nilsson, L. Modeling Zinc Sulfhydryl Interactions in Zinc Fingers. *Int. J. Quantum Chem.* **2001**, *83*, 230−244.
(19) Aqvist, J.; Warshel, A. Computer Simulation of the Initial Proton Transfer Step in Human Carbonic Anhydrase I. *J. Mol. Biol.* **1992**, *224*, 7−14.
(20) Hoops, S. C.; Anderson, K. W.; Merz, K. M. Force Field Design for Metalloproteins. *J. Am. Chem. Soc.* **1991**, *113*, 8262−8270.
(21) Peters, M. B.; Yang, Y.; Wang, B.; Molnar, L. F.; Weaver, M. N. Structural Survey of Zinc-Containing Proteins and Development of the Zinc AMBER Force Field (ZAFF). *J. Chem. Theory Comput.* **2010**, *6*, 2935−2947.
(22) Wu, R. B.; Lu, Z. Y.; Cao, Z. X.; Zhang, Y. K. A Transferable Nonbonded Pairwise Force Field to Model Zzinc Interactions in Metalloproteins. *J. Chem. Theory Comput.* **2011**, *7*, 433−443.
(23) Sakharov, D. V.; Lim, C. Zn Protein Simulations Including Charge Transfer and Local Polarization Effects. *J. Am. Chem. Soc.* **2005**, *127*, 4921−4929.
(24) Li, W. F.; Zhang, J.; Wang, J.; Wang, W. Metal-Coupled Folding of Cys2His2 Zinc-Finger. *J. Am. Chem. Soc.* **2008**, *130*, 892−900.
(25) Sakharov, D. V.; Lim, C. Force Field Including Charge Transfer and Local Polarization Effects: Application to Proteins Containing Multi/Heavy Metal Ions. *J. Comput. Chem.* **2009**, *30*, 191−202.
(26) Li, W. F.; Zhang, J.; Su, Y.; Wang, J.; Qin, M.; Wang, W. Effects of Zinc Binding on the Conformational Distribution of the Amyloid-β Peptide Based on Molecular Dynamics Simulations. *J. Phys. Chem. B* **2007**, *111*, 13814−13821.
(27) Miller, Y.; Ma, B. Y.; Nussinov, R. Zinc Ions Promote Alzheimer *A*β Aggregation via Population Shift of Polymorphic States. *Proc. Natl. Acad. Sci. U.S.A.* **2010**, *107*, 9490−9495.
(28) Wise-Scira, O.; Xu, L.; Perry, G.; Coskuner, O. Structures and Free Energy Landscapes of Aqueous Zinc(II)-Bound Amyloid-β (1−40) and Zinc(II)-Bound Amyloid-β (1−42) with Dynamics. *J. Biol. Inorg. Chem.* **2012**, *17*, 927−938.
(29) Kaminski, G. A.; Jorgensen, W. L. Host-Guset Chemistry of Rotaxanes and Catenanes: Application of A Polarizable All-Atom Force Field to Cyclobis (Paraquat-p-Phenylene) Complexes with Disubstituted Benzenes and Biphenyls. *J. Chem. Soc., Perkin Trans.* **1999**, *2*, 2365−2375.
(30) Kitaura, K.; Morokuma, K. A New Energy Decomposition Scheme for Molecular Interactions within the Hartree-Fock Approximation. *Int. J. Quantum Chem.* **1976**, *10*, 325−340.
(31) Lee, Y. M.; Lim, C. Physical Basis of Structural and Catalytic Zn-Binding Sites in Proteins. *J. Mol. Biol.* **2008**, *379*, 545−553.
(32) Andreini, C.; Bertini, I.; Cavallaro, G. Minimal Functional Sites Allow a Classification of Zinc Sites in Proteins. *PloS One* **2011**, *6*, e26325.
(33) Frisch, M. J.; Trucks, G. W.; Schlegel, H. B.; Scuseria, G. E.; Robb, M. A.; Cheeseman, J. R.; Montgomery, J. A.; Vreven, J. T.; Kudin, K. N.; Burant, J. C.; et al. *Gaussian 03*, revision D.01; Gaussian, Inc.: Wallingford, CT, 2004.
(34) Garmer, D. R.; Gresh, N. A. Comprehensive Energy Component Analysis of the Interaction of Hard and Soft Dications with Biological Ligands. *J. Am. Chem. Soc.* **1994**, *116*, 3556−3567.
(35) MacKerell, J. A. D.; Bashford, D.; Bellott, M.; Dunbrack, R.; Evanseck, J. D.; Field, M. J.; Fischer, S.; Gao, J.; Guo, H.; Ha, S.; et al. All-Atom Empirical Potential for Molecular Modeling and Dynamics Studies of Proteins. *J. Phys. Chem. B* **1998**, *102*, 3586−3616.
(36) Babu, C. S.; Lim, C. Empirical Force Fields for Biologically Active Divalent Metal Cations in Water. *J. Phys. Chem. A* **2006**, *110*, 691−699.
(37) Maple, J. R.; Cao, Y. X.; Damm, W.; Halgren, T. A.; Kaminski, G. A.; Zhang, L. Y.; Friesner, R. A. A Polarizable Force Field and Continuum Salvation Methodology for Modeling of Protein-Ligand Interactions. *J. Chem. Comput.* **2005**, *1*, 694−715.
(38) Swart, M.; Snijders, J. G.; Duijnen, P. T. V. Polarizabilities of Amino Acid Residues. *J. Comput. Methods Sci. Eng.* **2004**, *4*, 419−425.
(39) Miller, K. J. Additivity Methods in Molecular Polarizability. *J. Am. Chem. Soc.* **1990**, *112*, 8533−8542.
(40) Johnson, W. R.; Kolb, D.; Huang, K.-N. *At. Data Nucl. Data Tables* **1983**, *28*, 333.
(41) Niesar, U.; Corongiu, G.; Clementi, E.; Kneller, G. R.; Bhattacharya, D. K. Molecular Dynamics Simulations of Liquid Water Using the NCC Ab Initio Potential. *J. Phys. Chem.* **1990**, *94*, 7949−7956.

(42) Mackerell, A. D.; Feig, M. J. R.; Brooks, C. L., III. Extending the Treatment of Backbone Energetics in Protein Force Fields: Limitations of Gas-Phase Quantum Mechanics in Reproducing Protein Conformational Distributions in Molecular Dynamics Simulations. *J. Comput. Chem.* **2004**, *25*, 1400−1415.
(43) Phillips, J. C.; Braun, R.; Wang, W.; Gumbart, J.; Tajkhorshid, E.; Willa, E.; Chipot, C.; Skeel, R. D.; Kale, L.; Schulten, K. Scalable Molecular Dynamics with NAMD. *J. Comput. Chem.* **2005**, *26*, 1781−1802.
(44) Feig, M. Kinetics from Implicit Solvent Simulations of Biomolecules as a Function of Viscosity. *J. Chem. Theory Comput.* **2007**, *3*, 1734−1748.
(45) Brunger, A.; Brooks, C. L., III; Karplus, M. Stochastic Boundary Conditions for Molecular Dynamics Simulations of ST2 Water. *Chem. Phys. Lett.* **1984**, *105*, 495−500.
(46) Dominy, B. N.; Brooks, C. L., III. Development of A Generalized Born Model Parameterization for Proteins and Nucleic Acids. *J. Phys. Chem. B* **1999**, *103*, 3765−3773.
(47) Weiser, J.; Shenkin, P. S.; Still, W. C. Approximate Atomic Surfaces from Linear Combinations of Pairwise Overlaps (LCPO). *J. Comput. Chem.* **1999**, *20*, 217−230.
(48) Weiser, J.; Weiser, A. A.; Shenkin, P. S.; Still, W. C. Neighbor-List Reduction: Optimization for Computation of Molecular Van Der Waals and Solvent-Accessible Surface Areas. *J. Comput. Chem.* **1998**, *19*, 797−808.
(49) Stikoff, D.; Sharp, K. A.; Honig, B. Accurate Calculation of Hydration Free-Energies Using Macroscopic Solvent Models. *J. Phys. Chem.* **1994**, *98*, 1978−1988.
(50) Qiu, D.; Shenkin, P. S.; Hollinger, F. P.; Still, W. C. The GB/SA Continuum Model for Solvation: A Fast Analytical Method for the Calculation of Approximate Born Radii. *J. Phys. Chem. A* **1997**, *101*, 3005−3014.
(51) Gilson, M. K.; Honig, B. Calculation of the Total Electrostatic Energy of a Macromolecular System: Solvation Energies, Binding Energies, and Conformational Analysis. *Proteins* **1988**, *4*, 7−18.
(52) Schaefer, M.; Karplus, M. A Comprehensive Analytical Treatment of Continuum Electrostatics. *J. Phys. Chem.* **1996**, *100*, 1578−1599.
(53) Humphrey, W.; Dalke, A.; Schulten, K. VMD-Visual Molecular Dynamics. *J. Mol. Graphics* **1996**, *14*, 33−38.
(54) Ryde, U. Carboxylate Binding Modes in Zinc Proteins: A Theoretical Study. *Biophys. J.* **1999**, *77*, 2777−2787.
(55) Dudev, T.; Lim, C. Metal Binding and Selectivity in Zinc Proteins. *J. Chin. Chem. Soc.* **2003**, *50*, 1093−1102.
(56) Istrate, A. N.; Tsvetkov, P. O.; Mantsyzov, A. B.; Kulikova, A. A.; Kozin, S. A.; Makarov, A. A.; Polshakov, V. I. NMR Solution Structure of Rat *Aβ* (1−16): Toward Understanding the Mechanism of Rat's Resistance to Alzheimer's Disease. *Biophys. J.* **2012**, *102*, 136−143.